

Strengthening and Mechanical Properties of SiC and Graphite Reinforced Al6061 Hybrid Nanocomposites Processed Through Ultrasonically Assisted Casting Technique

A. Prasad Reddy¹  · P. Vamsi Krishna¹ · R. N. Rao¹

Received: 3 October 2018 / Accepted: 14 May 2019 / Published online: 31 May 2019
© The Indian Institute of Metals - IIM 2019

Abstract Al6061 alloy-based hybrid nanocomposites reinforced with 2wt% SiC and x wt% of graphite ($x = 0, 0.5, 1, 1.5, 2$ and 3) nanoparticles are fabricated through ultrasonically assisted casting technique. Microstructure, phases, grain size and fracture surfaces of the hybrid nanocomposites are studied to understand the mechanical properties. Microstructural studies revealed the uniform distribution of SiC and graphite nano-reinforcements in the matrix. The small-scale clusters appeared in the microstructure with the increase in graphite nanoparticles. The grain size, density, hardness and ultimate tensile strength of hybrid nanocomposites decreased with the rise of graphite in the composite material. The yield strength of the hybrid nanocomposites increased with increase in graphite up to 2 wt% and then decreased. SiC and graphite dual phase nanoparticles' strengthening effect on yield strength was theoretically evaluated using various strengthening mechanisms including porosity effect. Enhancement of yield strength in hybrid nanocomposite due to strengthening mechanisms followed the trend $\Delta\sigma_{\Delta CTE} > \Delta\sigma_{\text{Orowan}} > \Delta\sigma_{\text{HP}} > \Delta\sigma_{\text{load}}$. The predicted yield strength of hybrid nanocomposites obtained using the modified Clyne model and quadratic summation model were close to the experimental values. Fracture surfaces of hybrid nanocomposites exhibited brittle fracture with interdendritic cracking, stepwise facets and particle pull out with the increase in graphite content in the matrix.

Keywords Hybrid metal matrix nanocomposites · Strengthening mechanisms · Grain refinement · Microstructure · Fractography

1 Introduction

Aluminium-based materials are widely used in various automobile, structural, defence and aerospace applications due to their extreme properties [1]. The total weight and cost of structural or automobile assembly get reduced due to its lightweight [2]. It is noticed that the mechanical properties of aluminium-based materials are improved by reinforcing micron and nano-sized hard ceramic particles [3]. Researchers reported the improvement in strength and reduction in ductility with the micro particle ceramic reinforcements in aluminium-based composites. But, ceramic nanoparticles reinforced aluminium composites exhibited high strength along with better ductility compared to micron sized reinforced aluminium composites [3]. Ceramic reinforcements such as silicon carbide (SiC) [3], alumina (Al₂O₃) [4], graphite [5], graphene (GNPs) [4], boron carbide (B₄C) [6] and titanium boride (TiB₂) [7] are used in composites fabrication. Among them, SiC reinforcement particles have been proved to have good compatibility with aluminium and its alloys. The SiC particles reinforced aluminium composites result in good mechanical properties. Especially in the automobile sector, the Al-SiC composites are used as pistons, cylinder liners, and truck bodies, bearing surfaces, brake components, gears and connecting rods [8]. Mechanical properties are very important in all these applications.

Many reports have specified various methods for fabrication of aluminium-based composites. These are classified as solid-state and liquid-state methods. In solid-state

✉ A. Prasad Reddy
aprasadreddy43@gmail.com

¹ Department of Mechanical Engineering, NIT Warangal, Warangal, Telangana 506004, India

method, mostly powder metallurgy route is used for micron-sized or nano-sized reinforced aluminium composites. In powder metallurgy route, nanoparticles are dispersed better in the matrix up to 2 V_f %. However, more than 2 V_f % addition results in the formation of agglomeration and non-uniform dispersion in the matrix [9]. Liquid-state fabrication methods such as stir casting, melt infiltration, squeeze casting and compocasting are established for micron-sized particle reinforced aluminium-based composites. These methods are not effective for uniform dispersion of nanoparticles in the aluminium alloy matrix; formation of nanoparticle clusters and poor wettability are observed in the matrix. Researchers suggested the ultrasonically assisted casting method which improves the particle distribution and decreases the formation of nanoparticle clusters in the matrix. During the ultrasonication process, the acoustic waves produce a tensile force which tends to the formation of tiny cavities in the molten metal. These tiny cavities expand and compress during cycles and helps the nano-reinforcement clusters to disintegrate into nanoparticles due to the variation of pressure gradient with local high temperatures. During this process, gases are removed from the molten metal, grain refinement occurs, homogeneity increases and reduces segregation. The mechanical properties of Al-SiC nanocomposites processed through ultrasonically assisted casting technique are improved. Qiang et al. [10] fabricated Al-SiC nanocomposites by varying the volume fraction of SiC reinforcements in the aluminium matrix. SiC nanoparticles were distributed uniformly in the matrix and dendritic sizes were reduced. The strength of Al-SiC nanocomposites improved due to SiC nanoparticle strengthening effect. Harichandran et al. [11] produced Al-B₄C-h-BN hybrid nanocomposites through ultrasonically assisted casting method. Significant improvement in tensile strength was observed in Al-6wt% B₄C nanocomposites and better elongation was identified in case of Al-2wt% B₄C-2wt% h-BN hybrid nanocomposites. Mechanical and tribological properties were improved for B₄C ceramic particles reinforced aluminium-based composites fabricated through ultrasonication process [12]. Afsaneh et al. [13] manufactured Al-Al₂O₃-TiB₂ hybrid nanocomposites through ultrasonically assisted casting technique. The strength of hybrid nanocomposites improved due to the grain refinement and Orowan strengthening mechanism. Kannan et al. [14] fabricated Al7075-Al₂O₃-h-BN hybrid nanocomposites through ultrasonically assisted casting and molten salt processing technique and subjected to T6 condition. Hardness, tensile strength and elongation of the hybrid nanocomposites were improved. Shulin et al. [15] fabricated Al-SiC nanocomposites through ultrasonic vibration method. SiC nanoparticles were processed through dry ball milling and diluted in molten metal. Ultrasonication

process improved the uniform dispersion of SiC nanoparticles in the matrix, and grain size was reduced. Many research works proved that the mechanical properties were improved through ultrasonically assisted casting technique.

Dual phases of SiC and graphite nano-reinforcement particles play a major role in particle strengthening in case of hybrid nanocomposites. Many studies reported that the mechanical properties reduce for graphite reinforced aluminium composites. Studies on SiC and graphite nano-reinforced aluminium hybrid nanocomposites are seldom found. It is necessary to understand the strengthening effect of SiC and graphite nano-reinforcements, reinforcement particle dispersion, microstructural variations, and mechanical properties and fracture surface of hybrid nanocomposites. There is a scope for Al-SiC-graphite hybrid nanocomposites in various tribological systems such as automobile industry and aircraft applications including the engine block, engine valves, pistons and cylinders due to their good sliding characteristics [16]. In the present study, Al6061 alloy, Al6061-2wt% SiC- x wt% graphite ($x = 0, 0.5, 1, 1.5, 2$ and 3) are fabricated through ultrasonically assisted casting technique. The effect of various strengthening mechanisms such as load-bearing effect, Orowan strengthening effect, thermal dislocation mismatch effect and Hall-Petch effect are studied. The theoretical yield strength of hybrid nanocomposites is predicted using various models and compared with the experimental values.

2 Materials and Methods

Bharat Aerospace Metals, India, supplied the commercial grade of Al6061 alloy in the T6 condition. The elemental composition of Al6061 alloy was Mg (0.93), Si (0.52), Fe (0.25), Cu (0.18), Mn (0.14), Zn (0.09), Cr (0.07), Ni (0.03), Ti (0.01) and Al (balance). Beta silicon carbide (SiC) nanopowder of average particle size 50 nm was procured from US Research Nanomaterials, Inc., USA. Graphite particles of average particle size 500 nm were supplied by Mknano, M K Impex Corp., Canada. The SiC and graphite particles were analysed under transmission electron microscopy (TEM) to ensure the size of the particles shown in Fig. 1.

The schematic view of ultrasonically assisted casting set-up used for manufacturing of Al6061 alloy, Al6061-2wt% SiC (named as 2NC), Al6061-2wt% SiC- x wt% graphite ($x = 0.5, 1, 1.5, 2$ and 3) (named as 1HNC, 2HNC, 3HNC, 4HNC and 5HNC) hybrid nanocomposites is presented in Fig. 2. The experimental set-up consists of an electrical resistance heating furnace, thermocouples, ultrasonic unit, air compressor for cooling, ultrasonic generator, furnace control unit and argon supply unit.

Fig. 1 TEM micrographs of nanoparticles **a** SiC, **b** graphite

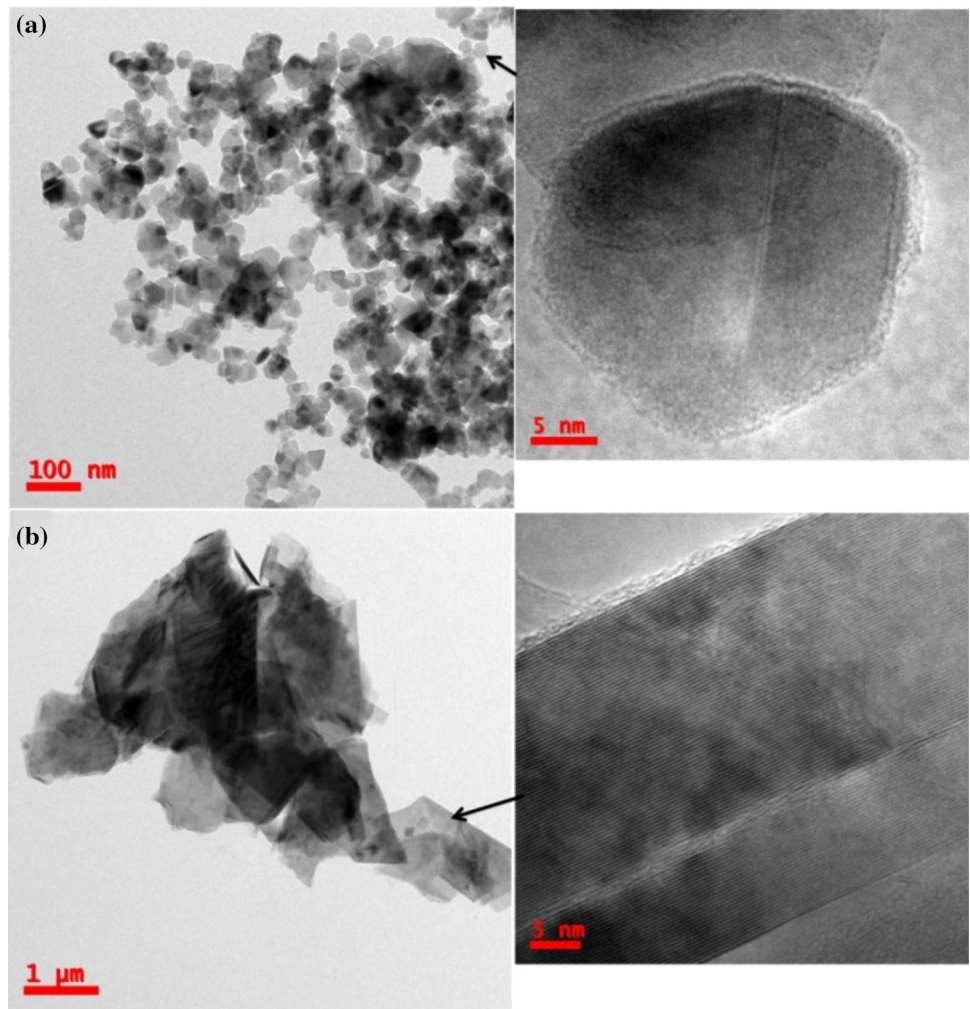
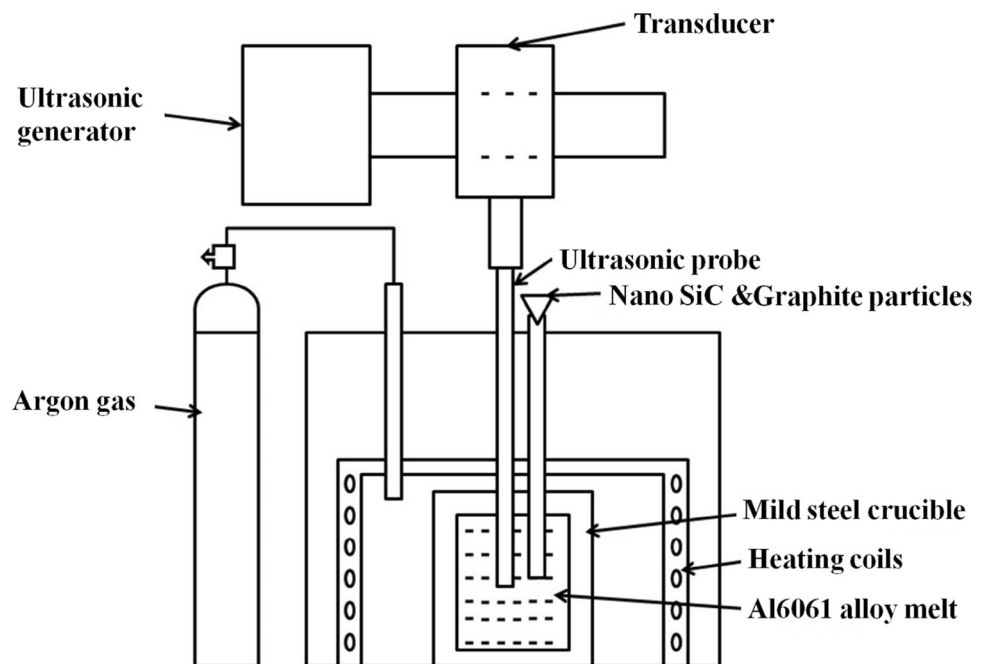


Fig. 2 Schematic diagram of ultrasonically assisted stir casting set-up



Ultrasonic horn of 20 mm diameter made up of Ti-10Al-4 V alloy coated with zirconia (ZrO_2) was used for sonication. A commercially available pure Al6061 alloy ingot of 500 g was melted in a steel crucible at 750 °C. The steel crucible present is of inner diameter 70 mm, thickness 8 mm and length 120 mm. The nano-sized SiC and graphite particles were enclosed with aluminium foil and preheated up to 550 °C. Upon reaching the temperature of steel crucible to 780 °C, the preheated foil was fed into the Al6061 alloy molten metal. Initial mixing of nano-sized SiC and graphite particles in the molten metal was done using mechanical stirrer for 10 min. The ultrasonication probe was preheated to 780 °C and inserted into the Al6061 alloy molten melt to a depth of about 25 mm for 5 min.

The density of AA6061 alloy (2.7 g/cm^3) [1], nano SiCp (3.218 g/cm^3) [5] and graphite (2.266 g/cm^3) [5] was collected from the literature. The experimental density of the samples was examined at room temperature (25 °C) by the Archimedes principle using a precision digital electronic weighing balance of 0.0001 g accuracy. Microhardness of Al6061 alloy and hybrid nanocomposite materials was measured using Vickers microhardness tester. The indenter shape with a square-based pyramidal diamond of face angles 136° , 250 gf test load and 10 s dwell time was used for microhardness study. The Vickers microhardness experiments were conducted according to ASTM: E384-08 standard [17]. Six readings were taken; mean and standard deviation were included in measurement of hardness values. Hybrid nanocomposite samples were characterized initially using a scanning electron microscope (SEM) of TESCAN Make Model Vega LMU 3. The samples were etched with 25 ml methanol (CH_2O), 25 ml hydrochloric acid (HCl), 25 ml nitric acid (HNO_3) and one drop of hydrofluoric acid (HF) for 40 s. The optical microscope Quosmo make model QX-4RT was used for microstructural analysis. The average grain size of the hybrid nanocomposites was measured using the mean linear intercept method. Tensile specimens were prepared by using ASTM E8/E8 M standard [18]. Tensile test of hybrid nanocomposites was conducted with a strain rate of 10^{-3} /s using an electromechanical tensile testing machine. Tensile experiments were repeated for the same composition for five times to get accurate results on each hybrid nanocomposite specimen, and subsequently, each of them was averaged. After performing the tensile test, the fracture surfaces of hybrid nanocomposite specimens were analysed under SEM.

3 Results and Discussions

3.1 Microstructural and XRD Analysis

Figure 3 shows the optical micrographs of various materials processed through ultrasonically assisted stir casting, i.e. Al6061 alloy, 2NC nanocomposite, 1HNC, 2HNC, 3HNC, 4HNC and 5HNC hybrid nanocomposites. The grain refinement is observed in the microstructure by keeping SiC as constant with increase in graphite content in the Al6061 alloy matrix. The optical micrographs reveal the variation in grain size of hybrid nanocomposites compared to Al6061 alloy. Variation of the average grain size is represented in Fig. 4. The average grain size of different materials is 120 μm for Al6061 alloy, 47 μm for 2NC, 42 μm for 1HNC, 35 μm for 2HNC, 25 μm for 3HNC, 20 μm for 4HNC and 15 μm for 5HNC, respectively. The microstructure of different hybrid nanocomposites reveal that the average grain size reduces with increase in graphite nano-reinforcements in the Al6061 alloy. The reduction in average grain size compared to base alloy are 58%, 61%, 71%, 79%, 83% and 88% for 2NC, 1HNC, 2HNC, 3HNC, 4HNC and 5HNC, respectively. This may be attributed to the increase in graphite nano-reinforcements in molten metal, which act as heterogeneous nucleation sites and increase the rate of nucleation. Grain refinement occurs mainly based on the reinforcement particle size, wt% of nanoparticles and ultrasonic cavitation effect [19].

The grain size of the matrix decreases with the reduction in reinforcement particle size and increasing wt% of nanoparticles. This may be due to the higher incidence of grain boundary pinning effect that reduces grain growth [20]. Figure 5 represents the SEM micrographs of Al6061 alloy, 2NC nanocomposite, and 1HNC, 2HNC, 3HNC, 4HNC and 5HNC hybrid nanocomposites. From Fig. 5b, the grayish-white SiC nanoparticles are present in Al6061 alloy matrix and are uniformly distributed in the matrix. However, few smaller SiC particle clusters are observed in the matrix. Figure 5c–g reveals that SiC and graphite reinforcements are dispersed uniformly in the Al6061 alloy matrix. However, small-scale clusters appear in the microstructure with the rise in graphite quantity in the matrix.

XRD analysis of Al6061 alloy, SiC, graphite, 2NC nanocomposite, 1HNC, 2HNC, 3HNC, 4HNC and 5HNC hybrid nanocomposites is presented in Fig. 6. The properties of the hybrid nanocomposites are influenced by the nature of the reinforcing material. The various phases of hybrid nanocomposites are recognized through JCPDS software in XRD studies. XRD pattern for 2NC nanocomposite reveals the SiC (111), Al (111), Al (022), Al (311) and Al (222) miller indices for different intensity

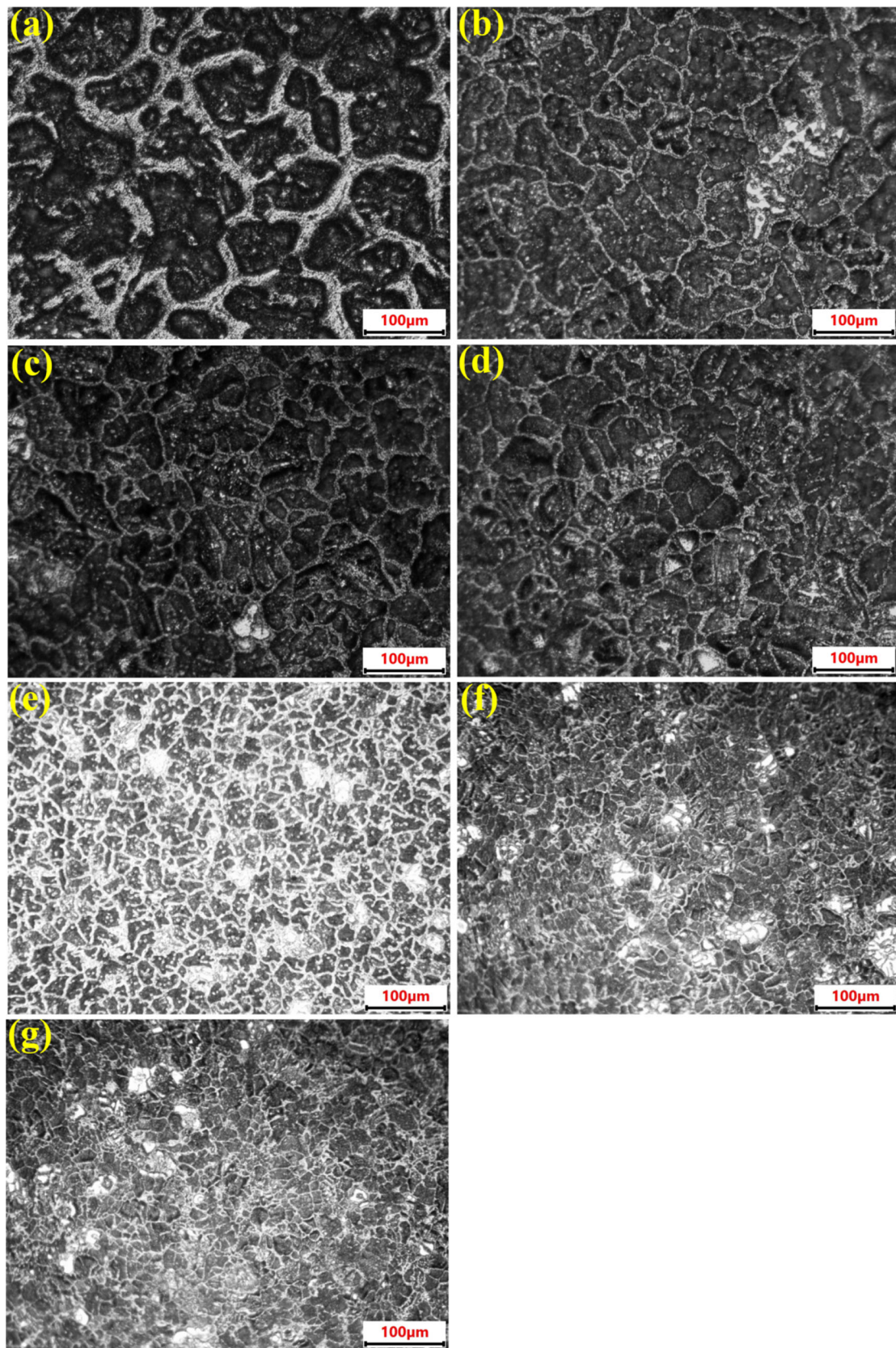


Fig. 3 Optical images of various materials **a** Al6061 alloy, **b** 2NC, **c** 1HNC, **d** 2HNC, **e** 3HNC, **f** 4HNC and **g** 5HNC

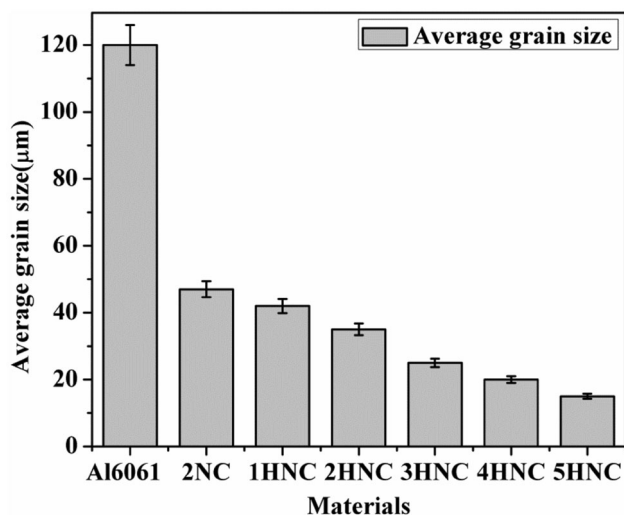


Fig. 4 Variation of average grain size of hybrid nanocomposites

of peak. It is observed that the intensity of SiC peak is small due to its lower quantity in the matrix. The XRD pattern for 3HNC, 4HNC and 5HNC hybrid nanocomposites at different intensities of peaks are exhibited at C (002), SiC (111), Al (111), Al (020), Al (022), Al (311) and Al (222). The intensity peaks are lower for graphite and SiC due to their lower content in the matrix. The intensity of peaks of graphite does not appear in 1HNC and 2HNC hybrid nanocomposite due to its lower content in the matrix.

3.2 Density of Hybrid Nanocomposites

Theoretical density, experimental density and porosity of Al6061 alloy, 2NC nanocomposite, 1HNC, 2HNC, 3HNC, 4HNC and 5HNC hybrid nanocomposites are represented in Fig. 7. The theoretical and experimental density increase for 2NC nanocomposites and then decrease for hybrid nanocomposites. It is noticed that the density of hybrid nanocomposites reduces due to the presence of a lower density graphite powder compared to the nanocomposite and base material. The porosity of hybrid nanocomposites increases with the increase in nano-reinforcements in the Al6061 alloy matrix. It is due to the rise in contact surface area of graphite nanoparticles with air and quantity of air present in the molten metal during ultrasonic processing. Similarly, the rise in the porosity of nanocomposites is reported with the increase in weight per cent in the matrix [1].

3.3 Mechanical Properties

The average Vickers microhardness of Al6061 alloy, 2NC nanocomposite, 1HNC, 2HNC, 3HNC, 4HNC and 5HNC hybrid nanocomposites are shown in Fig. 8. The microhardness of the composites increases with increase in SiC and graphite nano-reinforcement particles in the matrix. The enhancement of microhardness for 2NC nanocomposite, 1HNC, 2HNC, 3HNC, 4HNC and 5HNC hybrid

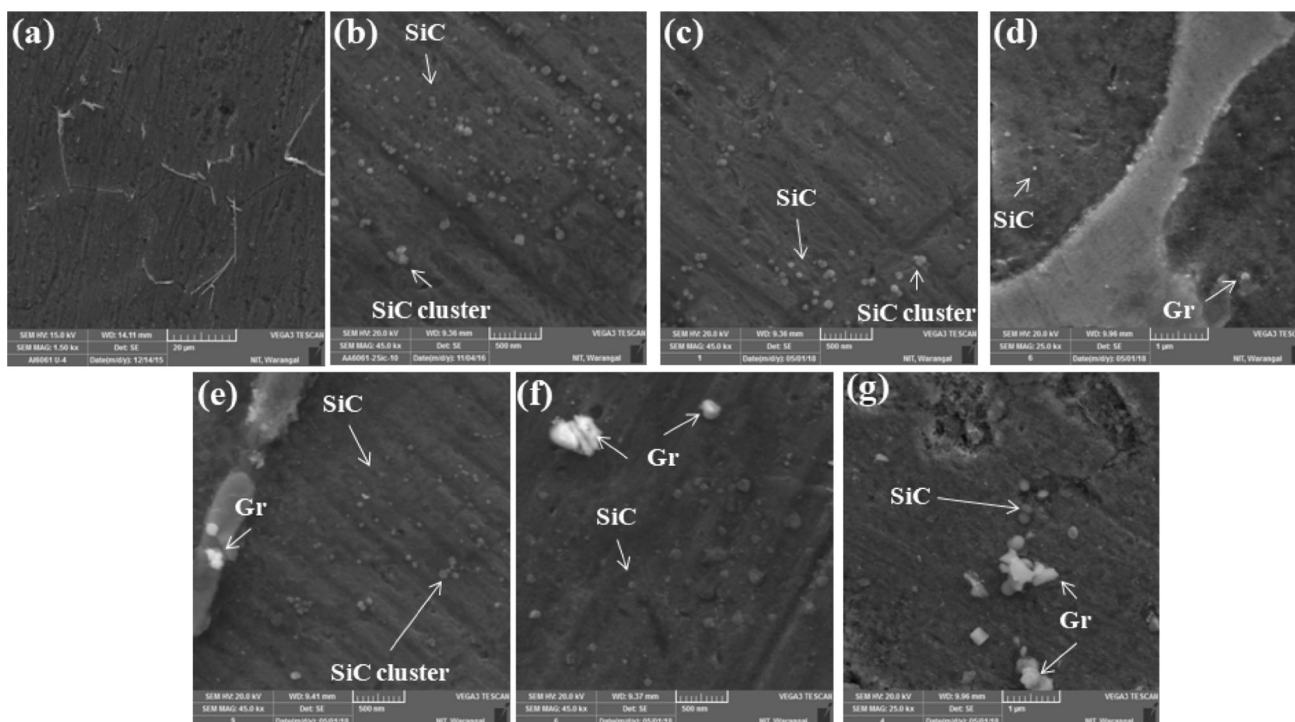


Fig. 5 SEM images of materials **a** Al6061 alloy, **b** 2NC nanocomposite, **c** 1HNC, **d** 2HNC, **e** 3HNC, **f** 4HNC and **g** 5HNC hybrid nanocomposites

Fig. 6 XRD of pure Al6061 alloy, 2NC, 1HNC, 2HNC, 3HNC, 4HNC and 5HNC hybrid nanocomposites

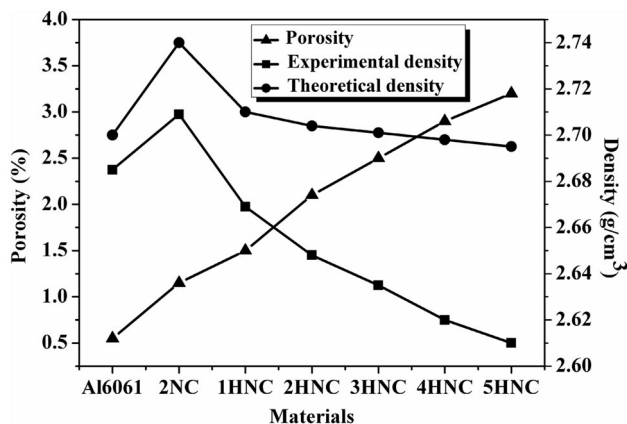
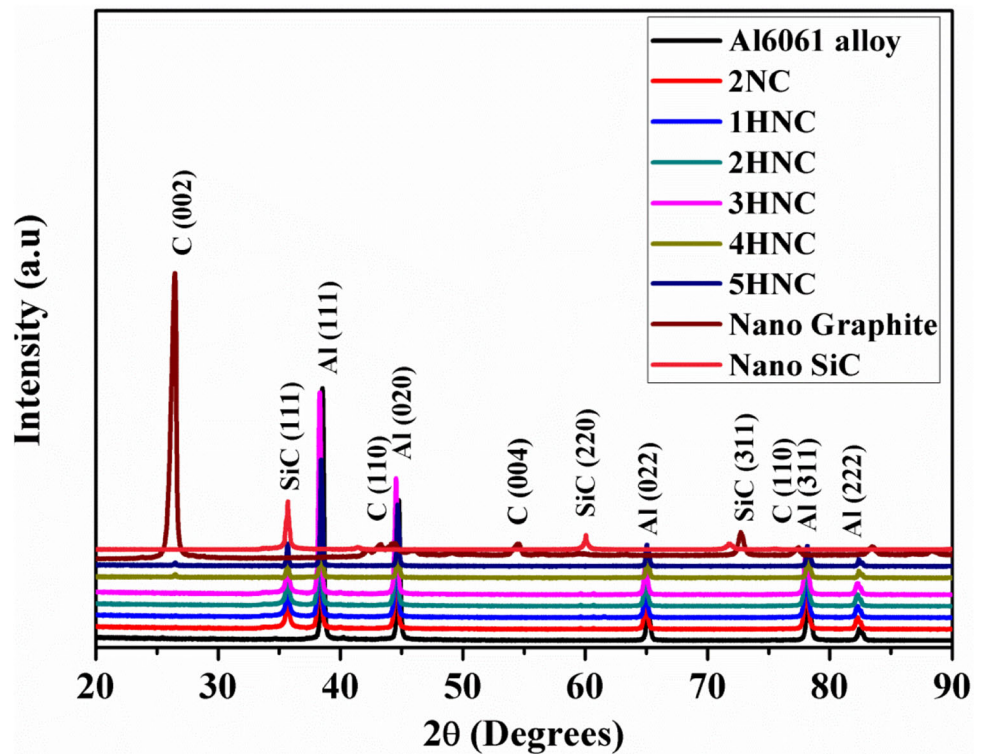


Fig. 7 Density of Al6061 alloy and its hybrid nanocomposites

nanocomposites compared to base alloy are 75%, 71%, 67%, 64%, 60% and 46%, respectively. The increase in microhardness can be due to the mixed effect of grain size reduction, SiC nanoparticle’s strengthening effects. Microhardness of hybrid nanocomposites increases compared to base alloy and decreases compared to nanocomposite. The reduction in microhardness of the hybrid nanocomposite can be due to the presence of graphite. The graphite being soft allotrope of carbon and solid lubricant, it will ease the grain movement along slip planes due to its weak Van der Waals forces between parallel thin plates [21].

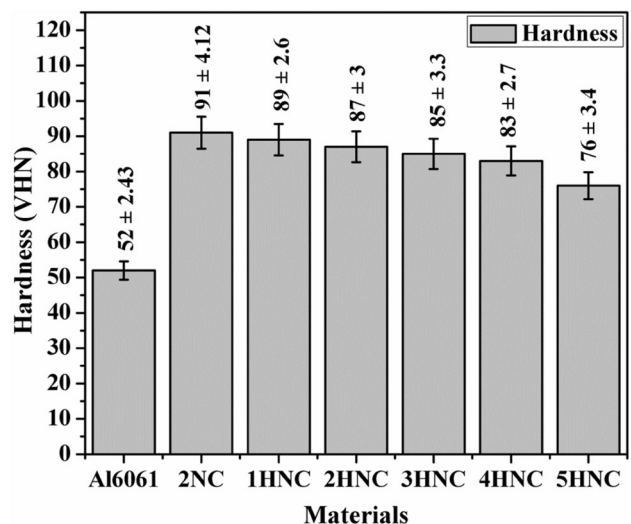


Fig. 8 Microhardness of Al6061 alloy, nanocomposite and hybrid nanocomposites

Figure 9 depicts the tensile test results conducted on Al6061 alloy, 2NC nanocomposite, and 1HNC, 2HNC, 3HNC, 4HNC, and 5HNC hybrid nanocomposites. The variation of strength properties is presented in Fig. 10. It is observed that the yield strength and ultimate tensile strength of 2NC nanocomposite compared to Al6061 alloy are increased by 206% and 79%, respectively. It is observed that the yield strength increases by 209% for 1HNC, 218% for 2HNC, 227% for 3HNC, 240% for 4HNC

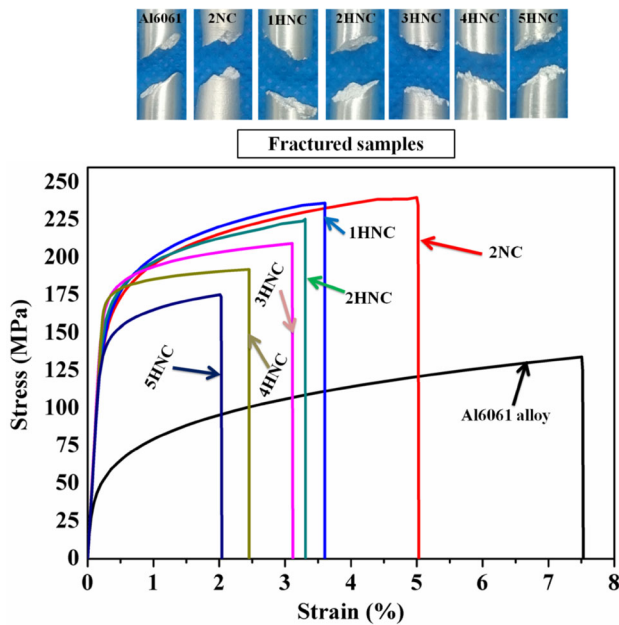


Fig. 9 Stress-strain curves of Al6061 alloy, 2NC nanocomposite and its hybrid nanocomposites

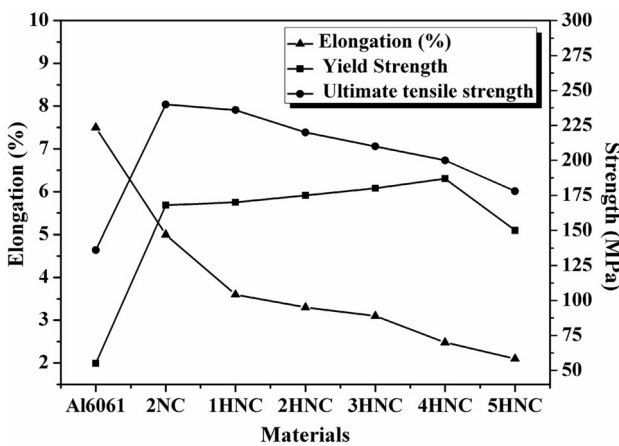


Fig. 10 Strength properties of Al6061 alloy, 2NC and its hybrid nanocomposites

and 173% for 5HNC hybrid nanocomposites compared to base alloy. Enhancement of yield strength is attributed to the rise of dislocation density, uniform distribution and combined strengthening effect of nano-reinforcements in the matrix. The enhancement of the yield strength increases up to 4HNC and suddenly decreases for 5HNC hybrid nanocomposite. This can be attributed to the formation of nano-reinforcement clusters and higher amount of graphite in the alloy matrix. The results specify that the ultimate tensile strength increases by 76% for 1HNC, 64% for 2HNC, 57% for 3HNC, 49% for 4HNC and 33% for 5HNC hybrid nanocomposites compared to base alloy. The addition of graphite content to the 2NC nanocomposite decreases the enhancement of ultimate tensile strength. The

percentage of elongation is 7.5 for Al6061 alloy, 5 for 2NC nanocomposite, 3.6 for 1HNC, 3.3 for 2HNC, 3.1 for 3HNC, 2.5 for 4HNC and 2.1 for 5HNC hybrid nanocomposites. The elongation of the nanocomposites decreases with increase in graphite nano-reinforcements in the base alloy. This may be attributed to the increase in brittleness with the increase in nano-reinforcements in the matrix. However, the increase in nano-reinforcements in the matrix repels the plastic flow of the matrix and decreases the ductility, which results in the reduction in the elongation percentage [22].

3.4 Strengthening Mechanisms

The yield strength of Al6061 alloy-based hybrid nanocomposites is influenced by SiC and graphite nano-reinforcements. There are various strengthening mechanisms implemented to evaluate the yield strength of nanocomposites, i.e. Hall–Petch effect [23], Orowan strengthening mechanism [24], Dislocation mismatch effect [25], load-bearing effect [26] and porosity effect [27]. The grain size is refined with the addition of SiC and graphite nano-reinforcements in the Al6061 alloy matrix. The grain size refinement enhances the yield strength of the hybrid nanocomposites [28]. Hall–Petch developed a relationship between grain size and yield strength of nanocomposites. The reduction in grain size of Al6061 alloy increases the yield strength of the hybrid nanocomposite according to the Hall–Petch relationship. The enhancement of the yield strength of hybrid nanocomposite as compared to the Al6061 alloy due to grain refinement is as follows [23]:

$$\Delta\sigma_{HP} = k \left[\frac{1}{\sqrt{d_c}} - \frac{1}{\sqrt{d_m}} \right] \tag{1}$$

where d_m is the average grain size of Al6061 alloy matrix, d_c is the average grain size of SiC and graphite reinforced Al6061 hybrid nanocomposites, and k is equal to 74 MPa $\mu\text{m}^{1/2}$ [29]. The SiC and graphite second phase nanoparticles can act as obstacles to the dislocation’s movement and thus enhance the yield strength of the hybrid nanocomposites [30].

The Orowan strengthening effect due to the combination of SiC and graphite nanoparticles is described as follows [31]:

$$\Delta\sigma_{Orowan} = 0.13G_m b_m \left[\frac{\ln\left(\frac{d_{SiC}}{2b_m}\right)}{\tau_{SiC}} + \frac{\ln\left(\frac{d_{graphite}}{2b_m}\right)}{\tau_{graphite}} \right] \tag{2}$$

$$\tau_{SiC} = d_{SiC} \left(\left(\frac{1}{2V_{SiC}} \right)^{\frac{1}{3}} - 1 \right) \tag{3}$$

$$\tau_{Gr} = d_{\text{graphite}} \left(\left(\frac{1}{2V_{\text{graphite}}} \right)^{\frac{1}{3}} - 1 \right) \tag{4}$$

where $\Delta\sigma_{\text{Orowan}}$ is the change in yield strength due to Orowan effect, G_m is shear modulus of alloy, V_{SiC} is volume fraction of SiC nano-reinforcements, V_{graphite} is volume fraction of graphite nano-reinforcements, b_m is the magnitude of burgers vector of matrix material, d_{SiC} is the average diameter of the SiC nano-reinforcement, d_{graphite} is average diameter of the graphite nano-reinforcement, τ_{SiC} is the average interparticle spacing of SiC, and τ_{graphite} is the average interparticle spacing of graphite.

The large difference of coefficient of thermal expansion between matrix and graphite nano-reinforcements induces the thermal mismatch strengthening effect during cooling of the molten metal from the initial fabrication conditions. The induced thermal stresses near the interface around the nano-reinforcement particles are sufficient for plastic strain in the alloy matrix. Therefore, the increment in thermal stress due to the geometrically mismatched dislocations $\Delta\sigma_{\text{CTE}}$ is obtained from the empirical relation [31].

$$\Delta\sigma_{\text{CTE}} = \beta G_m b_m (\rho^{\text{CTE}})^{\frac{1}{2}} \tag{5}$$

$$\rho^{\text{CTE}} = \frac{A\Delta T}{b_m} \left[\frac{(\alpha_m - \alpha_{\text{SiC}})V_{\text{SiC}}}{d_{\text{SiC}}(1 - V_{\text{SiC}})} + \frac{(\alpha_m - \alpha_{\text{graphite}})V_{\text{graphite}}}{d_{\text{graphite}}(1 - V_{\text{graphite}})} \right] \tag{6}$$

where $\Delta\sigma_{\text{CTE}}$ is change in yield strength due to thermal mismatch effect, β is a constant equal to 1.25 [32], b_m is the magnitude of burgers vector of matrix material, G_m is the shear modulus of matrix, ρ^{CTE} is dislocation density, V_{SiC} is volume fraction of SiC nano-reinforcements, V_{graphite} is volume fraction of graphite nano-reinforcements, A is constant equal to 12, d_{SiC} is average SiC particle size, d_{graphite} is average graphite particle size, $(\alpha_m - \alpha_{\text{SiC}})$ is the difference of thermal expansion coefficient between the alloy matrix and SiC nano-reinforcement particle, $(\alpha_m - \alpha_{\text{graphite}})$ is difference of thermal expansion coefficient between the alloy matrix and graphite nano-reinforcement particle, and ΔT is the temperature change from the stress-free homologous temperature to the room temperature. It is assumed that the dislocation punching starts at a stress-free homologous temperature of 0.59 value and which is in good agreement with previous studies by various researchers [1]. The melting point temperature of Al6061 alloy is ($T_{\text{mp}} = 855$ K), and the measured room temperature during casting process is ($T_{\text{room}} = 298$ K). During cooling from a high annealing temperature to a room temperature, the SiC, graphite particles and the matrix are stress-free by diffusion until stress-free homologous temperature is reached.

$$\frac{T_{\text{sf}}}{T_{\text{mp}}} = 0.59 \tag{7}$$

$$\frac{T_{\text{sf}}}{855} = 0.59$$

Therefore, $T_{\text{sf}} = 504$ K

$$\Delta T = T_{\text{sf}} - T_{\text{room}} = (504 - 298) \text{ K} = 206 \text{ K}$$

where T_{sf} is the stress-free homologous temperature and T_{room} is the room temperature.

The good interface bonding between SiC, graphite nano-reinforcements and the Al6061 alloy matrix makes the nano-reinforcements to contribute to the externally applied load. The load-bearing effect of nano-reinforcement particles is given by the following relation [31].

$$\Delta\sigma_{\text{load}} = 0.5(V_{\text{SiC}} + V_{\text{graphite}})\sigma_m \tag{8}$$

where $\Delta\sigma_{\text{load}}$ is a change in yield strength due to load-bearing effect, V_{SiC} is volume fraction of SiC nano-reinforcements, V_{graphite} is volume fraction of graphite reinforcement particles, and σ_m is yield strength of Al6061 alloy. The porosity of the metal matrix hybrid nanocomposites plays an important role on the yield strength. The porosity of the hybrid nanocomposites increases with the increase in volume fraction of the nano-reinforcement particles in the Al6061 alloy matrix that reduces the yield strength [27]. The porosity of hybrid nanocomposites may interrupt load balance between the nano-reinforcement particles and matrix material, which results in stress concentration, crack initiation and crack propagation. Based on the literature, f_p is the degradation factor represented as a function of porosity in the hybrid nanocomposites, which is as follows [27]:

$$f_p = 1 - e^{-np} \tag{9}$$

where n is empirical constant equal to 1.943 and p is porosity.

Strengthening contributions of the 2NC nanocomposite, 1HNC, 2HNC, 3HNC, 4HNC and 5HNC hybrid nanocomposites are presented in Table 1, which are calculated using the parameters given in Table 2. Various strengthening contributions of SiC nanoparticles are effectively more than that of graphite nanoparticles. This can be attributed to the addition of smaller sized SiC particles and increase in dislocation density in the matrix. Size factor also affects the yield strength of the matrix, whereas in this case, SiC nanoparticles are 10 times smaller than the graphite nanoparticles. The various strengthening effects are calculated for hybrid nanocomposites by fixing the SiC nanoparticle’s content in the Al6061 alloy matrix and by varying the graphite nanoparticle’s content. The Hall–Petch effect $\Delta\sigma_{\text{HP}}$ for 5HNC hybrid nanocomposite is more than 3.34, 2.64, 2.14, 1.53 and 1.27 times than 2NC nanocomposite, 1HNC, 2HNC, 3HNC and 4HNC hybrid

Table 1 Yield strength contribution from various strengthening mechanisms

Materials/strengthening mechanisms	2NC	1HNC	2HNC	3HNC	4HNC	5HNC
$\Delta\sigma_{HP}$ (MPa)	3.71	4.7	5.8	8.1	9.8	12.4
$\Delta\sigma_{load}$ (MPa)	0.47	0.63	0.79	0.95	1.2	1.5
$\Delta\sigma_{\Delta CTE}$ (MPa)	72.8	74.1	75.2	76.62	77.9	80.4
$\Delta\sigma_{Orowan}$ (MPa)	41.23	45.1	46.52	47.7	48.7	50.51

Table 2 Yield strength of hybrid nanocomposites are predicted using these parameters

Material	E (GPa)	G (GPa)	α ($10^{-6}/K$)	ν	b (nm)	d (nm)	V_f	ΔT (K)
β -SiC			4.5 [33]			50	0.01684	
Graphite			4.06 [34]			500		
Al6061 alloy	69	26	25.2 [29]	0.33 [29]	0.286 [1]			
Al6061/SiC								206
Al6061/graphite								206

ν is Poisson's ratio of Al6061 alloy matrix

nanocomposites, respectively. This can be attributed due to the decreased grain size of hybrid nanocomposites and combined strengthening effect of SiC and graphite nanoparticles in the matrix. The load-bearing effect $\Delta\sigma_{load}$ for 5HNC hybrid nanocomposites is more than 3.2, 2.4, 1.9, 1.6, and 1.3 times than 2NC nanocomposite, 1HNC, 2HNC, 3HNC and 4HNC hybrid nanocomposites, respectively. The Orowan effect $\Delta\sigma_{Orowan}$ for 5HNC hybrid nanocomposite is more than 1.23, 1.12, 1.08, 1.05 and 1 times than 2NC nanocomposite, 1HNC, 2HNC, 3HNC and 4HNC hybrid nanocomposites, respectively. The thermal dislocation mismatch effect $\Delta\sigma_{\Delta CTE}$ for 5HNC hybrid nanocomposite is more than 1.1, 1.08, 1.06, 1.05 and 1.03 times than 2NC nanocomposite, 1HNC, 2HNC, 3HNC and 4HNC hybrid nanocomposites, respectively. The contribution of load-bearing effect is much lower than the other strengthening mechanisms (Table 3). The enhancement of yield strength is more influenced by $\Delta\sigma_{\Delta CTE}$ followed by $\Delta\sigma_{Orowan}$, $\Delta\sigma_{HP}$ and $\Delta\sigma_{load}$, respectively.

3.5 Yield Strength Prediction Models

Different prediction models have been described for studying the enhancement of yield strength of nanocomposites, i.e. Ramakrishnan's model [35], Zhang and Chen model [36], Mirza and Chen model [27], modified Clyne model [27], arithmetic model [35], quadratic summation model [1], and compounding models [37]. Ramakrishnan introduced a model to predict yield strength as a function of load-bearing effect and dislocation mismatch effect. According to Ramakrishnan's model, the yield strength of the composite is given by the following relation [35].

$$\sigma_{ync} = (\sigma_m) \left(1 + \frac{\Delta\sigma_{load}}{\sigma_m} \right) \left(1 + \frac{\Delta\sigma_{\Delta CTE}}{\sigma_m} \right) \quad (10)$$

Zhang and Chen implemented yield strength prediction model as a function of Orowan effect, thermal mismatch effect and load-bearing effect. The rise in the yield strength of the hybrid nanocomposites can be described as follows [30]:

$$\sigma_{ync} = (\sigma_m) \left(1 + \frac{\Delta\sigma_{load}}{\sigma_m} \right) \left(1 + \frac{\Delta\sigma_{\Delta CTE}}{\sigma_m} \right) \left(1 + \frac{\Delta\sigma_{Orowan}}{\sigma_m} \right) \quad (11)$$

Mirza and Chen developed a model to predict the yield strength of hybrid nanocomposites including load-bearing effect, thermal dislocation mismatch effect, Orowan effect, Hall–Petch effect and porosity effect. Then, the yield strength of the hybrid nanocomposites is as given below [27]:

$$\sigma_{ync} = (\sigma_m) \left(1 + \frac{\Delta\sigma_{load}}{\sigma_m} - P \right) \left(1 + \frac{\Delta\sigma_{\Delta CTE}}{\sigma_m} \right) \left(1 + \frac{\Delta\sigma_{Orowan}}{\sigma_m} \right) \left(1 + \frac{\Delta\sigma_{HP}}{\sigma_m} \right) (e^{-nP}) \quad (12)$$

Srivastava et al. [1] suggested the quadratic summation model for prediction of the yield strength of nanocomposites. This model is proposed for micron sized particle reinforced composites. Several reports specify that the nanocomposite properties significantly improves and the assumptions for micron sized particles reinforced composites cannot be applied to nanocomposites. This model assumes that the total enhancement of yield strength is proportional to the sum of the squares of each

Table 3 Predicted and experimental yield strengths of hybrid nanocomposites

Materials/models	σ_{ync} (MPa)					
	2NC	1HNC	2HNC	3HNC	4HNC	5HNC
Ramakrishnan’s (Eq. 10)	129	131	132.1	134	136	139.1
Zhang and Chen (Eq. 11)	226	235	244	250.0	261	267
Mirza and Chen (Eq. 12)	232.7	247	253.4	254.4	255.2	243
Quadratic (Eq. 13)	139	142	144	146	147.4	151
Modified Clyne (Eq. 14)	143	147	150	154.3	158	164
Arithmetic (Eq. 15)	118.2	125	128.4	133.4	138	145
Compounding (Eq. 16)	241	258	270	287	302	327
Experimental value	168	170	175	180	187	150

strengthening effect under the square root. The yield strength of nanocomposites is theoretically calculated using Eq. (12) given below.

$$\sigma_{ync} = \sigma_m + \sqrt{\Delta\sigma_{HP}^2 + \Delta\sigma_{Orowan}^2 + \Delta\sigma_{\Delta CTE}^2 + \Delta\sigma_{load}^2} \tag{13}$$

Orowan and thermal mismatch effect play a major role in the increment of the yield strength of hybrid nanocomposites. Hall–Petch effect and the load-bearing effect are negligible compared to other strengthening mechanisms. Orowan and thermal mismatch strengthening mechanisms directly influence the yield strength of hybrid nanocomposites. So that it is required to take the sum of squares of Orowan and thermal mismatch effect under square root. Considering these two strengthening mechanisms under the square root is known as modified Clyne model [38].

$$\sigma_{ync} = \sigma_m + \Delta\sigma_{HP} + \Delta\sigma_{load} + \sqrt{\Delta\sigma_{Orowan}^2 + \Delta\sigma_{\Delta CTE}^2} \tag{14}$$

Summation of the contribution of each strengthening mechanism is known as arithmetic summation model. According to this model, the various strengthening effects act and independently contribute to the yield strength of the hybrid nanocomposites [38].

$$\sigma_{ync} = \sigma_m + \Delta\sigma_{HP} + \Delta\sigma_{Orowan} + \Delta\sigma_{\Delta CTE} + \Delta\sigma_{load} \tag{15}$$

According to compounding model, the enhancement of yield strength due to nano-reinforcements is multiplied to σ_m as shown in Eq. (16) below [39].

$$\sigma_{ync} = (\sigma_m) \left(1 + \frac{\Delta\sigma_{HP}}{\sigma_m}\right) \left(1 + \frac{\Delta\sigma_{load}}{\sigma_m}\right) \left(1 + \frac{\Delta\sigma_{\Delta CTE}}{\sigma_m}\right) \left(1 + \frac{\Delta\sigma_{Orowan}}{\sigma_m}\right) \tag{16}$$

The predicted yield strength of 2NC nanocomposite, 1HNC, 2HNC, 3HNC, 4HNC and 5HNC hybrid

nanocomposites is compared with the experimental results shown in Table 3. The predicted yield strength of hybrid nanocomposites obtained from the modified Clyne model and quadratic summation model is close to the experimental yield strength values. But there is a sudden decrement in yield strength for 5HNC hybrid nanocomposites. This is due to the presence of maximum amount of a porosity and nanoparticle cluster formation in the 5HNC hybrid nanocomposite.

3.6 Fractography

Figure 11 represents the fracture surfaces of Al6061 alloy, 2NC nanocomposite, and 1HNC, 2HNC, 3HNC, 4HNC and 5HNC hybrid nanocomposites. The fracture surface of Al6061 alloy as shown in Fig. 11a reveals grape-like dendrites in higher quantity, micro cracks, tear ridges, facets and tiny dimples in smaller quantity. The mode of fracture of Al6061 alloy is a ductile fracture (i.e. 45°). Figure 11b indicates that the 2NC nanocomposite fracture surface appears to have more tiny dimples in a smaller size and stepwise facets. The appearance of larger quantities of tiny dimples is an indication of ductile mode of fracture [40]. This ductile failure will be due to the nucleation of voids and voids growth. The voids grow up and form a crystalline boundary with the matrix and SiC nanoparticles. The formation of voids will spread into small dimples and finally cracks. Figure 11c shows the 1HNC hybrid nanocomposite fracture surface that reveals the smaller sized tiny dimples and more stepwise facets [17]. It can be seen that the number of tiny dimples can be observed and its size is reduced. The sudden reduction in the dimple size is an indication of lower ductility. This can be attributed due to the rise of nano-reinforcements particles in the matrix.

Figure 11d–f shows the SEM images of fracture surfaces of 2HNC, 3HNC and 4HNC hybrid nanocomposites. It reveals the plastic slip bonds, cleavage and stepwise

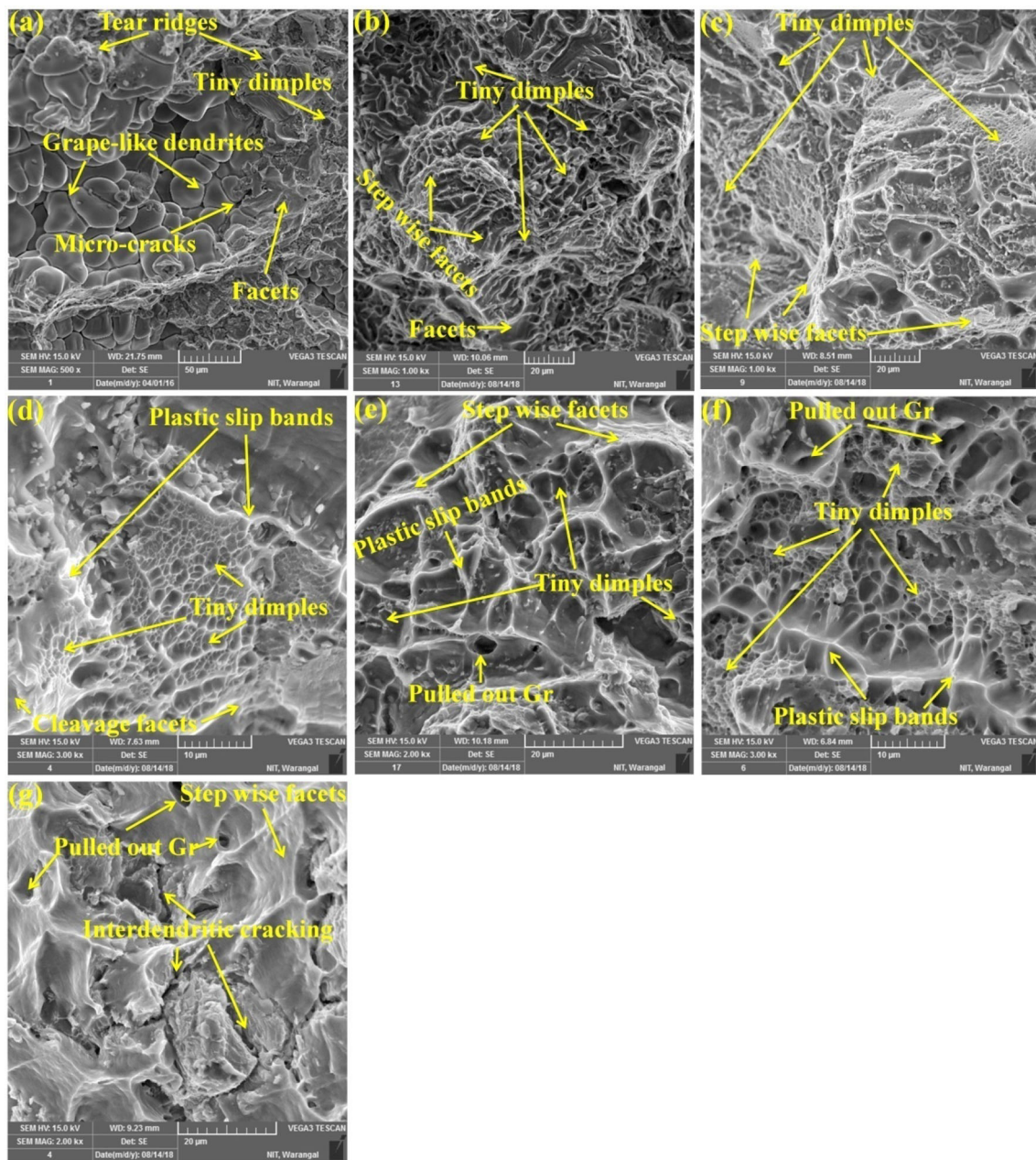


Fig. 11 SEM micrographs of fractured surfaces of materials **a** Al6061 alloy, **b** 2NC, **c** 1HNC, **d** 2HNC, **e** 3HNC, **f** 4HNC and **g** 5HNC

facets. It is observed that the nano-reinforcement particles are pulled out from the matrix. The appearance of more cleavage facets is an indication of ductile–brittle fracture mode. Figure 11g represents the SEM micrographs of the fracture surface of 5HNC hybrid nanocomposite exhibiting the interdendritic cracking, stepwise facets and particle pull outs. The interdendritic cracking is an indication of typical brittle fracture mode [41]. This is due to the rise of SiC and graphite nano-reinforcement clusters along the grain boundaries. However, the crack nucleation may be started along the grain boundaries and triple junctions

followed by their propagation along the weakest neighbour grains [42].

4 Conclusions

Different materials such as Al6061 alloy, 2NC nanocomposite, 1HNC, 2HNC, 3HNC, 4HNC and 5HNC are successfully produced through ultrasonically assisted casting technique. The following conclusions are drawn from the present study.

- SEM micrographs reveal the uniform distribution of SiC and graphite nano-reinforcements in the matrix. However, small-scale clusters appear in the microstructure with an increase in graphite.
- XRD pattern of hybrid nanocomposites exhibit the C and SiC peaks. The peaks have appeared at higher content of graphite reinforced Al6061/2SiC nanocomposites.
- Theoretical and experimental density increase for 2NC nanocomposite and then decrease for hybrid nanocomposites. It is noticed that the density of hybrid nanocomposites reduces due to the presence of a lower density graphite powder compared to the nanocomposite and base material. The porosity of hybrid nanocomposites increases with the increase in nano-reinforcements in the Al6061 alloy matrix.
- The enhancement of microhardness for 2NC nanocomposite, 1HNC, 2HNC, 3HNC, 4HNC, and 5HNC hybrid nanocomposites compared to base alloy are 75%, 71%, 67%, 64%, 60% and 46%, respectively. The increase in microhardness is due to the mixed effect of grain size reduction and SiC nanoparticle strengthening effects. The reduction in microhardness of the hybrid nanocomposite can be due to the presence of graphite.
- It is observed that the yield strength and ultimate tensile strength of 2NC nanocomposite compared to Al6061 alloy are increased by 206% and 79%, respectively. The yield strength increases by 209% for 1HNC, 218% for 2HNC, 227% for 3HNC, 240% for 4HNC and 173% for 5HNC hybrid nanocomposites compared to base alloy.
- Enhancement of yield strength value of the strengthening mechanisms follows the trend ($\Delta\sigma_{\Delta CTE} > \Delta\sigma_{\text{Orowan}} > \Delta\sigma_{\text{HP}} > \Delta\sigma_{\text{load}}$) for nanocomposites.
- The predicted yield strength of hybrid nanocomposites obtained from the modified Clyne model and quadratic summation model are close to the experimental values.
- Fracture surfaces of hybrid nanocomposites reveal the interdendritic cracking, stepwise facets and particle pull out. The increase in graphite content in the matrix results in brittle fracture mode. Cracks nucleate at triple junctions along the grain boundaries followed by their propagation along weakest neighbour grains.
- Boostani A F, Tahamtan S, Jiang Z Y, Wei D, Yazdani S, Azari R K, Mousavian R T, Xu J, Zhang X, Gong D, *Compos Part A Appl Sci Manuf* 68 (2015) 163.
- Fathy A, Oqail A A, Wagih A, *Ceram Int* (2018).
- Ravindran P, Manisekar K, Kumar S V, Rathika P, *Mater Des* 51 (2013) 456.
- Alexander R, Murthy T S R C, Ravikanth K V, Prakash J, Mahata T, Bakshi S R, Krishnan M, Dasgupta K, *Ceram Int* 44 (2018) 9838.
- Balci Ö, Ağaoğullari D, Gökçe H, Duman I, Öveçoğlu M L, *J Alloys Compd* 586 (2014) 32.
- Reddy A P, Krishna P V, Rao R N, *Proc Inst Mech Eng Part N J Nanomater Nanoeng Nanosyst* 231(4) (2017) 172.
- Govender G, Ivanchev L, Burger H, Mulaba A, Chikwande H, *J Compos Mat* (2012) 53.
- Li Q, Qiu F, Dong B X, Geng R, Lv M M, Zhao Q L, Jiang Q C, *Mater Sci Eng A* 735 (2018) 317.
- Harichandran R, Selvakumar N, *Int J Mech Sci* 144 (2018) 826.
- Harichandran R, Selvakumar N, *Arch Civ Mech Eng* 16 (2016) 158.
- Moghadam A D, Omrani E, Lopez H, Zhou L, Sohn Y, Rohatgi P K, *Mater Sci Eng A* 702 (2017) 321.
- Kannan C, Ramanujam R, *J Alloys Compd* 751 (2018) 193.
- Lü S, Xiao P, Yuan D, Hu K, Wu S, J. Mater. Sci. Technol. 34 (2018) 1617.
- Mavhungu S T, Akinlabi E T, Onitiri M A, Varachia F M, *Procedia Manuf* 7 (2017) 182.
- Reddy M P, Shakoor R A, Parande G, Manakari V, Ubaid F, Mohamed A M A, Gupta M, *Prog Nat Sci Mater Int* 27 (2017) 614.
- Gupta R, Chaudhari G P, Daniel B S S, *Compos Part B Eng* 140 (2018) 34.
- Eskin G I, Eskin D G, *Ultrason Sonochem* 10 (2003) 301.
- Khandelwal A, Mani K, Srivastava N, Gupta R, Chaudhari G P, *Compos Part B Eng* 123 (2017) 73.
- Sharma P, Sharma S, Khanduja D, *Part Sci Technol* 34 (2016) 22.
- Reddy A P, Krishna P V, Rao R N, *Proc Inst Mech Eng Part N J Nanomater Nanoeng. Nanosyst* 231 (2017) 172.
- Zhang X, Li S, Pan B, Pan D, Zhou S, Yang S, Jia L, Kondoh K, *J Alloys Compd* 764 (2018) 288.
- Aghdam M K H, Mahmoodi M J, Ansari R, *J Alloys Compd* 739 (2018) 177.
- Bisht A, Srivastava M, Kumar R M, Lahiri I, Lahiri D, *Mater Sci Eng A* 695 (2017) 28.
- Xiao P, Gao Y, Yang C, Liu Z, Li Y, Xu F, *Mater Sci Eng A* 710 (2018) 259.
- Mirza F A, Chen D L, *Materials (Basel)* 8 (2015) 5153.
- Chen B, Shen J, Ye X, Jia L, Li S, Umeda J, Takahashi M, Kondoh K, *Acta Mater* 140 (2017) 325.
- Srivastava N, Chaudhari G P, *Mater Sci Eng A* 651 (2016) 247.
- Zhang Z, Chen D L, *Mater Sci Eng A* 483–484 (2008) 152.
- Deng K, Shi J, Wang C, Wang X, Wu Y, Nie K, Wu K, *Compos Part A Appl Sci Manuf* 43 (2012) 1284.
- Park J G, Keum D H, Lee Y H, *Carbon N Y* 95 (2015) 698.
- Talwar D N, *Mater Sci Eng B Solid State Mater Adv Technol* 226 (2017) 9.
- Tsang D K L, Marsden B J, Fok S L, Hall G, *Carbon N Y* 43 (2005) 2906.
- Ramakrishnan N, *Acta Mater* 44 (1996) 77.
- Alizadeh M, Beni H A, *Mater Res Bull* 59 (2014) 294.
- Zadeh A S, *Mater Sci Eng A* 531 (2012) 118.
- Wang M, Chen D, Chen Z, Wu Y, Wang F, Ma N, Wang H, *Mater Sci Eng A* 590 (2014) 254.
- Kim C S, Sohn I, Nezafati M, Ferguson J B, Schultz B F, Gohari Z B, Rohatgi P K, Cho K, *J Mater Sci* 48 (2013) 4204.

References

- Srivastava N, Chaudhari G P, *Mater Sci Eng A* 724 (2018) 207.
- Zeng X, Yu J, Fu D, Zhang H, Teng J, *Vacuum* 155 (2018) 375.

40. Yao X, Zhang Z, Zheng Y F, Kong C, Quadir M Z, Liang J M, Chen Y H, Munroe P, Zhang D L, *J Mater Sci Technol* 33 (2017) 1030.
41. Ramkumar K R, Sivasankaran S, Alaboodi A S, *J Alloys Compd* 709 (2017) 141.
42. Ozkaya S, Canakci A, *Powder Technol* 297 (2016) 16.

Publisher's Note Springer Nature remains neutral with regard to jurisdictional claims in published maps and institutional affiliations.